Understanding the seismic disorder attribute and its applications

Satinder Chopra[1] and Kurt J. Marfurt[2]

Abstract

While reflections associated with conformal sedimentary layers are usually coherent and continuous, other reflections, such as mass-transport complexes, karst collapse, and salt, may appear to be quite chaotic, without any specific orientation. We also may see chaotic events that have little to do with the target geology but rather are artifacts due to variations in the overburden and surface or budget limitations resulting in a suboptimum acquisition program. While some of these artifact issues can be handled at the time of processing, a certain level of randomness remains in most seismic data volumes. Geologic features of interpretational interest, such as fault damage zones, unconformities, and gas chimneys, often have randomness associated with them. The published work on randomness describes techniques such as *cross correlation* which measures randomness associated with noise, the *chaos* attribute based on eigen-analysis of gradient covariance, and the *seismic disorder* attribute based on application of second derivative operators in the three axial directions in a 3D seismic volume. We apply the seismic disorder attribute to two different data sets and find that it is a useful attribute for assessing the signal-to-noise ratio and data quality, in addition to helping delineate damage zones associated with large faults and the interior of salt dome structures.

Introduction

Seismic data interpretation is based on the identification and geologic classification of seismic amplitude and reflector morphology. The morphology in stratigraphic interpretation includes the identification of conformal, onlapping, offlapping, hummocky, and chaotic reflector packages, ideally integrated within a sequence stratigraphic framework. In addition to the seismic reflections corresponding to simple stratigraphic deposition, tectonic deformation, or hydrocarbon accumulation, we often encounter seismic reflections that change abruptly in different directions, exhibiting no specific waveform shape, amplitude, or orientation. Such data configurations are referred to as *seismic disorder*, *randomness*, or *chaos*, which can represent either seismic or geologic noise or a combination of the two. Incoherent seismic noise is commonly associated with aliased noise that leaks into the stack array, insufficient near-surface corrections, inaccurate velocities, and migration operator aliasing. Incoherent geology includes mass-transport complexes, fault damage zones, and karst collapses. Finally, seismic noise that can be an indicator of the underlying geology includes salt domes where the internal reflectivity is anomalously low and overprinted by random seismic noise, and gas chimneys and overpressured zones where an inaccurate velocity results in suboptimum imaging. The seismic "disorder" attribute measures all these phenomena and either can provide geologic insight or quantify the amount of seismic noise in the data, which may be useful in subsequent risk analysis.

In some early attempts at studying randomness as it pertains to noise, Dash and Obaidullah (1970) described a cross-correlation method for determination of signal and noise statistics for two seismic traces. This means of estimating the coherent component of the seismic data is used by several interpretation software packages as input to subsequent spectral balancing operations. The deep crustal reflection seismology community used cross correlation to highlight the rather infrequent coherent reflectors. This technique also formed the basis of highlighting discontinuities in exploration seismic data leading to the first coherence attribute (Bahorich and Farmer, 1995).

Randen et al. (2001) introduced the chaos attribute that is based on the eigenanalysis of the 3 × 3 gradient structure tensor. If the first eigenvalue is large, the corresponding first eigenvector defines the normal to a local plane of constant amplitude waveforms. If the three eigenvalues are equal, the data are totally chaotic. Intermediate values of chaos indicate the degree of data organization. The chaos attribute is available in several commercial software packages.

A totally different approach to quantifying randomness is through the use of the gray-level co-occurrence matrix (GLCM) texture attributes (West et al., 2002; Gao, 2003; Chopra and Alexeev, 2005). The co-occurrence matrix is computed from a structurally aligned window of seismic amplitude and can measure both organized (linear, wavy, brick) and disorganized patterns. Specifically, the GLCM entropy attribute describes the degree of disorder in the data and yields large values for chaotic or noisy regions in the seismic data.

Al-Dossary et al. (2014) proposed the seismic disorder attribute, which is sensitive to chaotic reflection patterns and noisy areas and is relatively insensitive to more organized discontinuities such as faults and channel edges. The algorithm essentially cascades a second derivative in the inline, crossline, and time directions on a window of the computed power (or energy) of the data. This is equivalent to squaring the data and filtering it with a disorder filter given as

$$\mathbf{L} = \left\{ \begin{bmatrix} 1 & -2 & 1 \\ -2 & 4 & -2 \\ 1 & -2 & 1 \end{bmatrix} \begin{bmatrix} -2 & 4 & -2 \\ 4 & -8 & 4 \\ -2 & 4 & -2 \end{bmatrix}, \begin{bmatrix} 1 & -2 & 1 \\ -2 & 4 & -2 \\ 1 & -2 & 1 \end{bmatrix} \right\}. \quad (1)$$

The application of this algorithm to seismic data has two drawbacks in that it is sensitive to local average amplitude yielding low disorder values for chaotic zones with low amplitude, and it exhibits some dubious diagonal lines (Al-Dossary et al., 2014).

Ha and Marfurt (2014) modified the algorithm by dividing the seismic disorder attribute by the RMS amplitude of the windowed data such that now it can be written as:

[1]Arcis Seismic Solutions, TGS, Calgary.
[2]The University of Oklahoma, Norman.

$$Disorder = \frac{\mathbf{L} \cdot \mathbf{e}}{|\mathbf{L}| * |\mathbf{e}| + \varepsilon}, \qquad (2)$$

where **L** is defined in equation 1, **e** is a cube of amplitude energy, '.' indicates a triple inner product, $|\square|$ indicates RMS magnitude, and ε is a small additive constant that prevents division by zero in the computations.

When the seismic disorder attribute is computed along structural dip, the diagonal artifact is minimized. We show applications of the seismic disorder attribute to different types of features seen in 3D seismic data volumes and demonstrate the insight that can be gained therefrom.

Applications

Example 1

Our first example is a vertical slice through a good-quality 3D seismic volume acquired in northwest Alberta, Canada,

showing three picked reflectors (Figure 1). At the location of the fault indicated by yellow arrows, we expect the reflection amplitudes to be coherent with a single discontinuity for a simple fault and incoherent if there is a somewhat wider damage zone representing a suite of conjugate faults. At the shallower horizons above this fault, marked with magenta and blue arrows, we see more continuous reflectors that drape or flex over the deeper fault. Just above each of these two horizons, it may be difficult to assess the disorder or entropy in the data. In Figures 2 and 3, we exhibit the corresponding images through the entropy and disorder-attribute volumes. At the location of the fault (yellow arrows), the entropy is seen to be high as expected. In the regions 40 ms above horizons 1 and 2 marked by magenta and cyan arrows, the entropy and disorder values are also higher due to the lower coherency of the reflections. However, notice that the disorder attribute shows more distinct variation at these locations, as highlighted by the yellow hexagon. The seismic disorder attribute seems to convey information that is more easily interpretable.
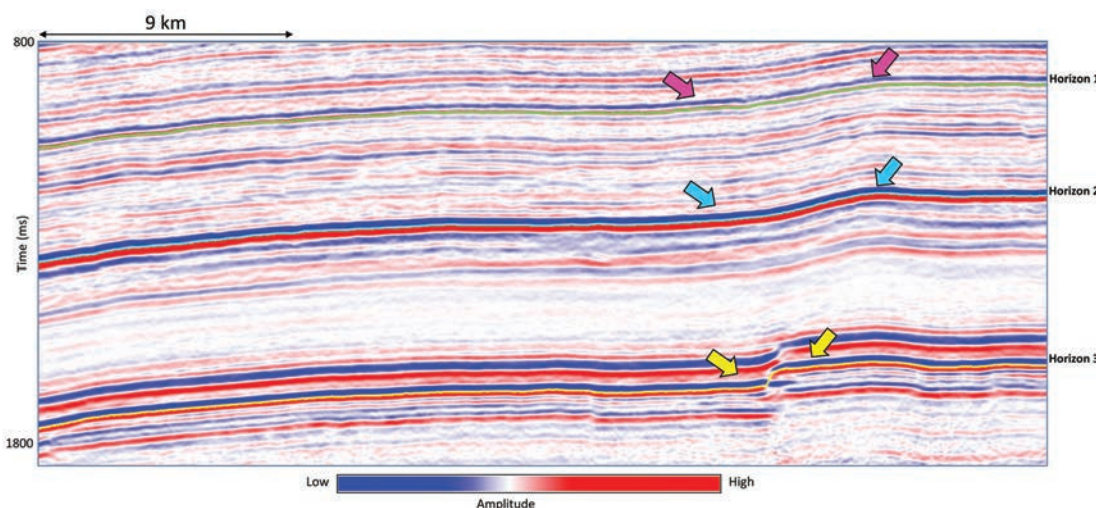

Figure 1. A segment of the inline from a 3D seismic volume. At the location of the fault indicated with yellow arrows, the seismic amplitudes are not expected to be coherent. At the location of the cyan and magenta arrows, just above the horizons, it may be difficult to ascertain the disorder or the entropy. Data courtesy of Arcis Seismic Solutions, TGS, Calgary.
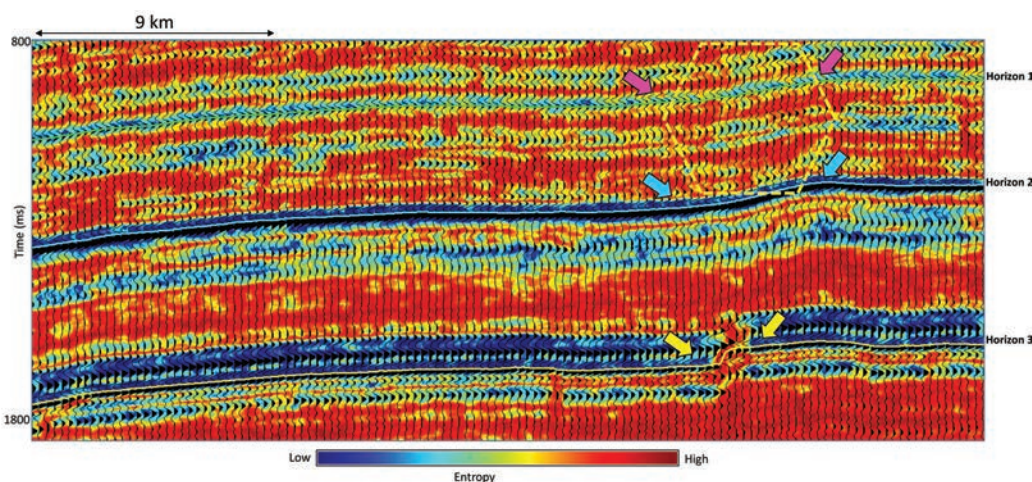

Figure 2. The same segment of the inline from a 3D seismic volume as shown in Figure 1 displays in wiggle and variable area overlaid on equivalent section from the GLCM entropy volume. Higher values of disorder are shown in bright orange. At the location of the fault indicated with yellow arrows, the entropy is quite high as expected. At the location of the blue and magenta arrows, just above the horizons, the entropy is higher and is open for interpretation. Every fourth trace has been plotted for the seismic data overlay. Data courtesy of Arcis Seismic Solutions, TGS, Calgary.

In Figure 4, we show a chair display with a vertical section through the seismic amplitude data and a strata slab through the seismic disorder attribute. Notice that the disorder-attribute values along the horizon — i.e., along the top of the strata slab — are all low as the horizon is quite smooth. At the location of the yellow arrow, we notice a streak of higher disorder-attribute values. This streak corresponds to the hypothesized damage zone seen at a lower level in Figures 1–3.

Figure 5 shows the same data as Figure 4 but now at a stratal slice slightly above the yellow horizon. Higher disorder values are clustered about the fault, suggesting a thinner damage zone. If we look at the equivalent chair display in Figure 6, where the vertical section is now through the seismic amplitude volume, there is a

sharp reflector displacement across the fault. But just below this level, we see higher values of the disorder attribute on both sides of the fault. We interpret these higher disorder values to be indicative of a damage zone associated with the main fault, but we need to evaluate the alternative hypothesis that the data are simply contaminated by noise. A question that might come up here is why would we expect a wide damage zone at the location in Figure 4 (far from fault) and a narrower zone near the fault (Figure 5), which seems counter-intuitive. We can explain it as follows:

At the deeper, yellow horizon shown in Figure 5, we see a discrete fault. Above this fault, the strain is accommodated either by a flexure, or by a system of fault splays; the details of both would fall below the seismic resolution of this data volume. In
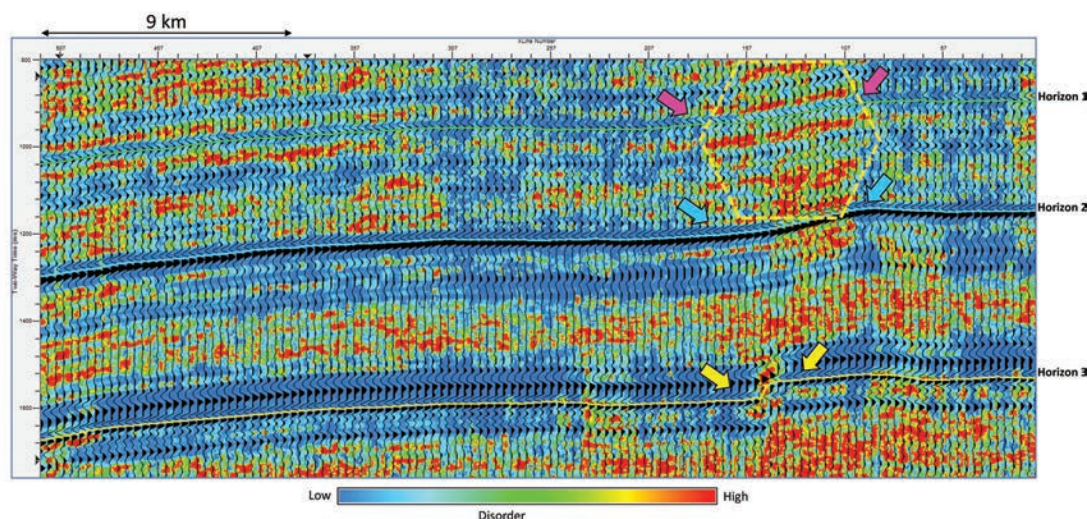

Figure 3. The same segment of the inline from a 3D seismic volume as shown in Figure 1 displays in wiggle and variable area overlaid on equivalent section through the disorder volume. Higher values of disorder are shown in bright orange. At the location of the fault indicated by yellow arrows, the disorder is quite high as expected. At the location of the cyan and magenta arrows, just above the horizons, the disorder is higher and is open for interpretation. Every fourth seismic trace has been plotted. Data courtesy of Arcis Seismic Solutions, TGS, Calgary.
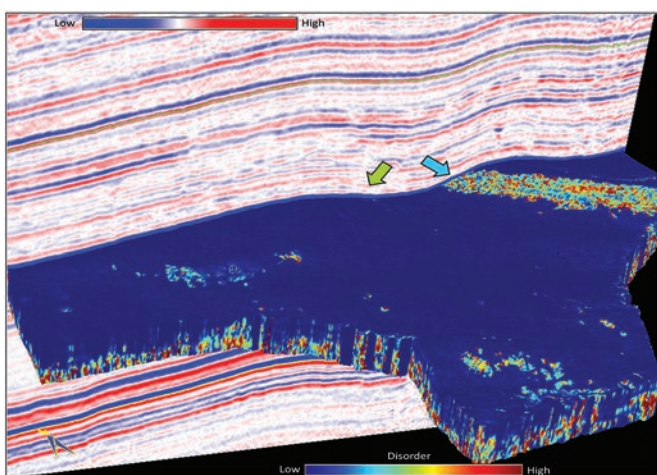

Figure 4. Vertical slice through seismic amplitude displayed with a strat cube along the cyan horizon through the disorder volume. The picked cyan horizon shown in Figure 3 is quite coherent and gives rise to a high-quality picked horizon. However, note that while coherent enough to autopick, the disorder attribute is quite low about the flexure associated with a deeper fault indicated by the cyan arrow. Note that there is no equivalent anomaly about the flexure indicated by the green arrow, not associated with a deeper fault. Data courtesy of Arcis Seismic Solutions, TGS, Calgary.
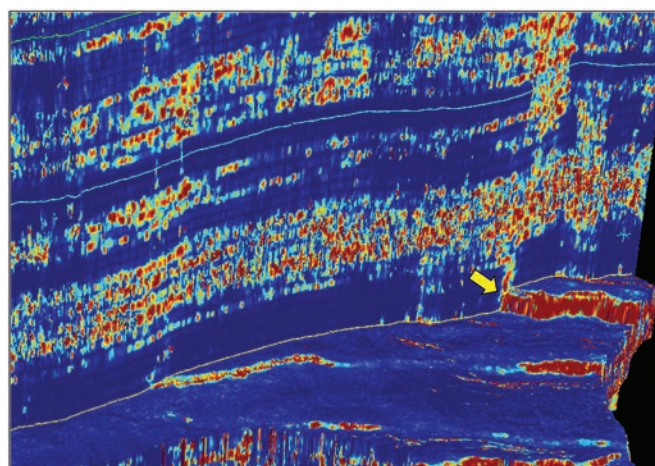

Figure 5. Vertical slice and strat cube along the deeper yellow horizon through the disorder volume. The picked yellow horizon shown in Figures 1–3 is coherent with low disorder except at the fault. Data courtesy of Arcis Seismic Solutions, TGS, Calgary.
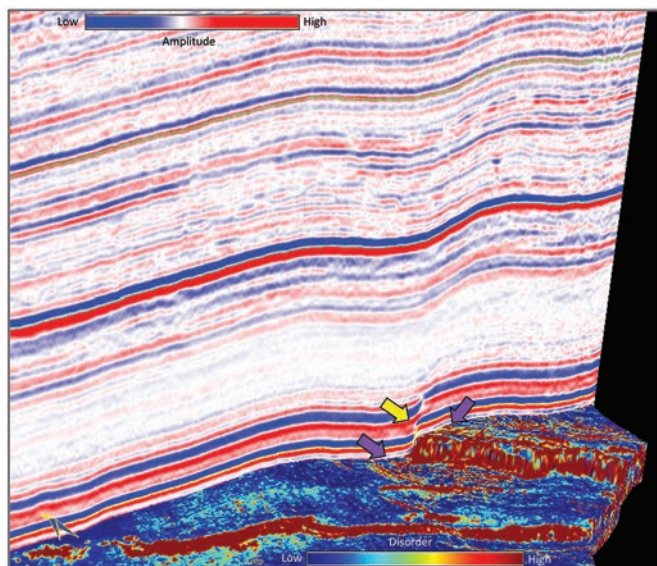
Figure 6. Vertical slice through seismic amplitude displayed with a strat cube 40 ms below the yellow horizon through the disorder volume. At the location of the yellow arrows in Figure 3, the horizon is coherent everywhere except at the location of the fault. The disorder-attribute values are all low elsewhere, except at the fault and a small width about both sides of the fault indicated by purple arrows. Data courtesy of Arcis Seismic Solutions, TGS, Calgary.

either case, we would expect subseismic resolution fractures to occur, giving rise to the diffuse disorder anomaly in Figure 4. Note that there is no accompanying disorder in the region indicated by the green arrow in Figure 4.

Preconditioning of seismic data and the seismic disorder attribute

In addition to computing attributes on the original data, we advise that the interpreter repeat the computation on the data after preconditioning. Common poststack data-conditioning processes include enhancing the signal-to-noise ratio and sharpening the discontinuities (Chopra and Marfurt, 2008) spectrally balancing or even boosting the frequency content of the data (Chopra et al., 2011), while less common prestack data-conditioning processes include interpolating missing traces, regularizing the offset and azimuth geometry (Chopra and Marfurt, 2013), and suppressing the acquisition footprint. Such processing of the seismic data often helps obtain better quality attributes, which can lead to more meaningful interpretation. The interpreter should always compare the seismic data before and after such data conditioning to make sure that more chaotic features of geologic interest are retained.

In Figures 7a and 7b, we show vertical slices through 3D seismic amplitude of and disorder computed from the original
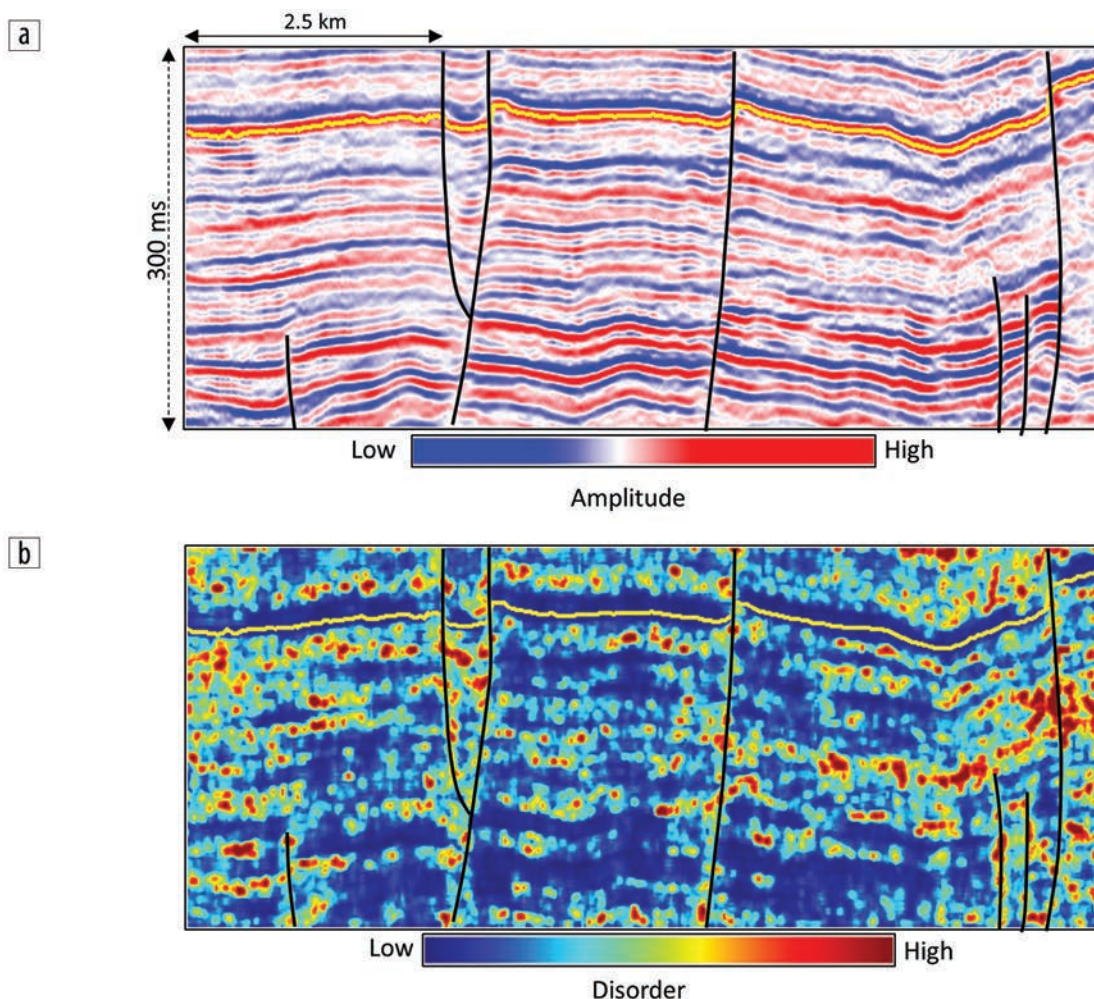

Figure 7. (a) Segment of a seismic section showing almost vertical faults. (b) Equivalent segment of the section in (a) from the seismic disorder attribute. The coherent zones exhibit low values of disorder while less coherent zones exhibit higher values of disorder. Data courtesy of Arcis Seismic Solutions, TGS, Calgary.
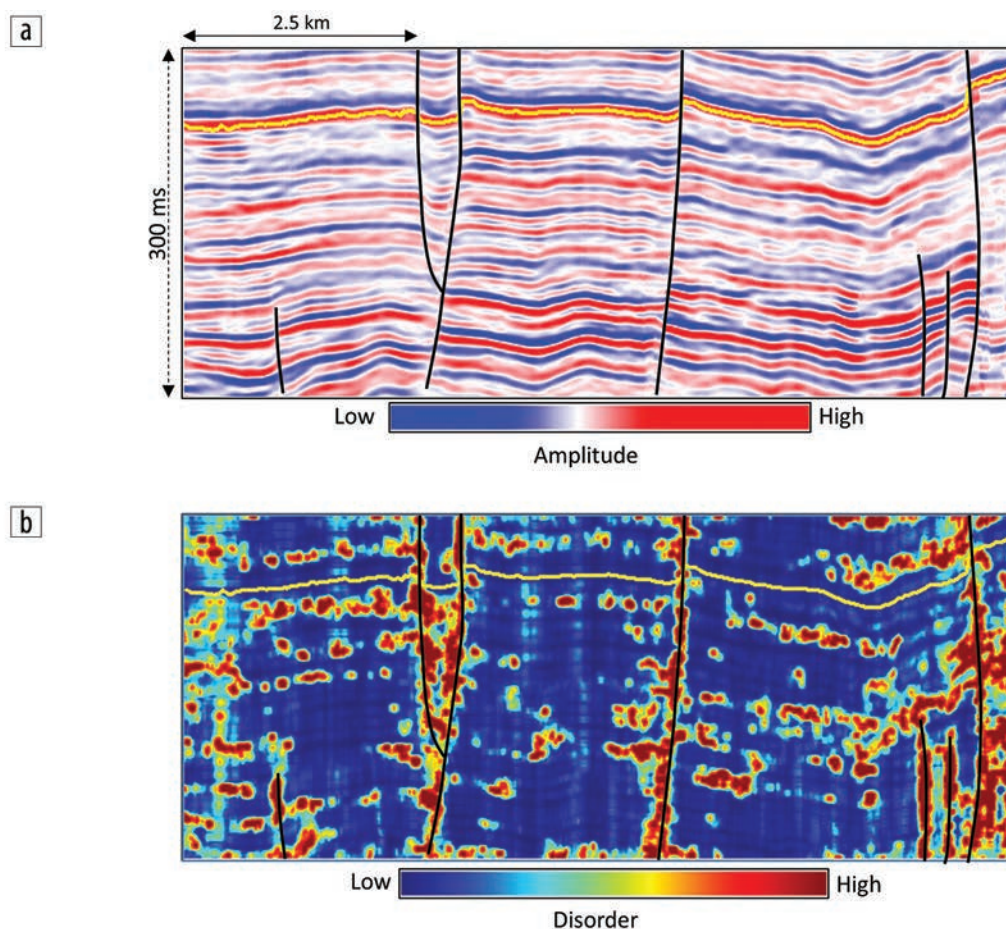
Figure 8. Equivalent segments of the data shown in Figure 7 but after preconditioning in terms of structure-oriented filtering and sharpening of discontinuities. Notice the fault planes exhibit higher disorder values in a background of low-disorder values. Data courtesy of Arcis Seismic Solutions, TGS, Calgary.
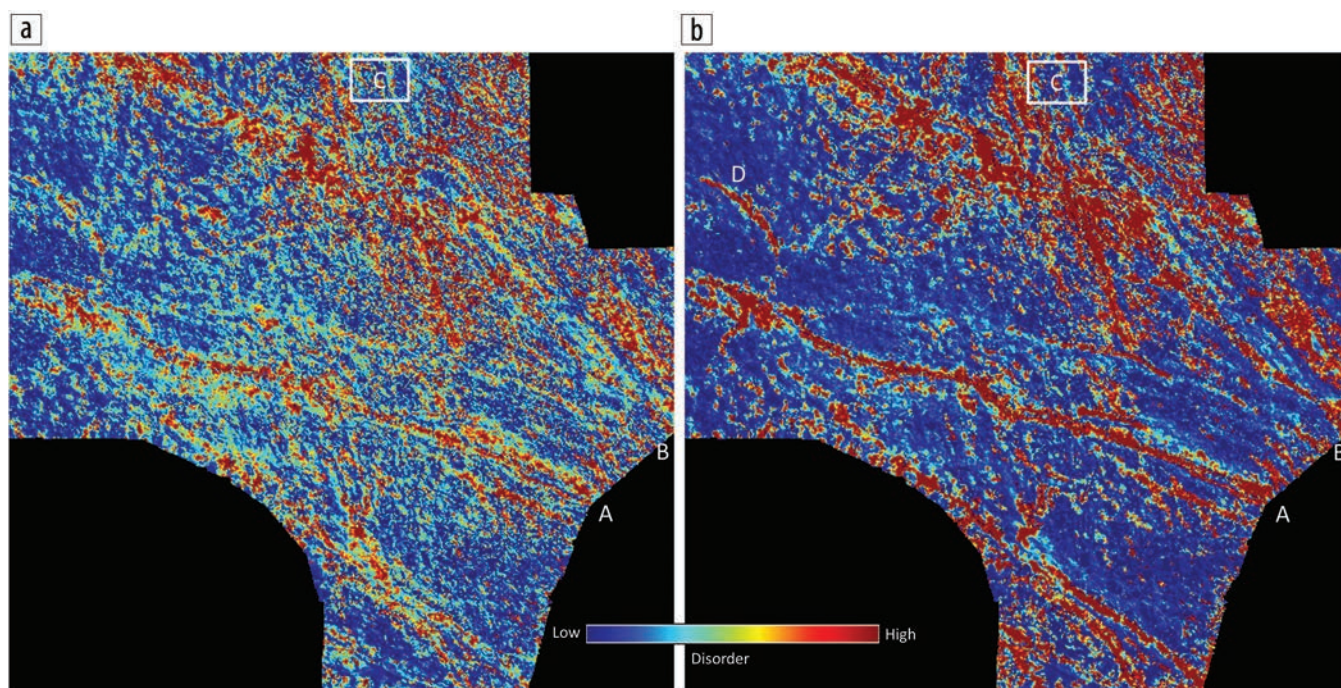

Figure 9. Strat slices 72 ms below a marker horizon close to 1600 ms through disorder volumes computed from the seismic data volume (a) before and (b) after pre-conditioning. Note that preconditioning reduces low-amplitude cross-cutting noise, resulting in more blue, while sharpening up discontinuities about the major faults, suggesting damage zones, results in more red. Data courtesy of Arcis Seismic Solutions, TGS, Calgary.
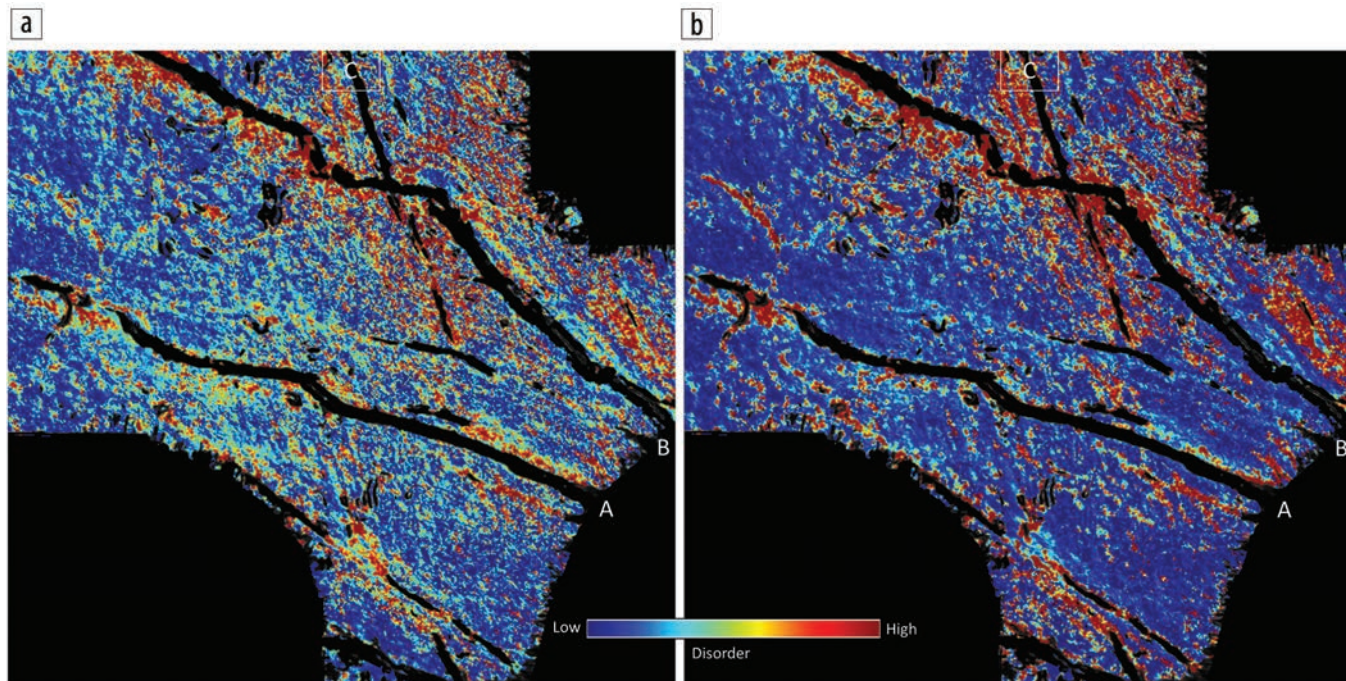
Figure 10. Strat slices 72 ms below a marker horizon close to 1600 ms from (a) disorder run on input seismic data and (b) from input seismic data after preconditioning. The coherence attribute has been overlaid on the two displays using transparency. Notice the low disorder values in the background and enhanced disorder lineaments indicating faults. Data courtesy of Arcis Seismic Solutions, TGS, Calgary.
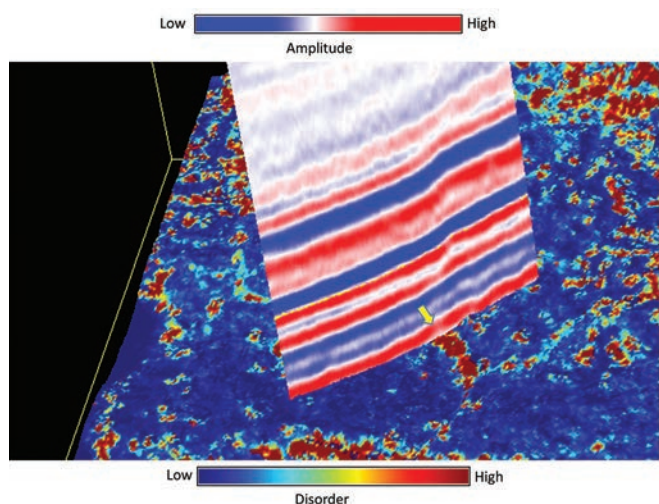

Figure 11. Strat slices 72 ms below a marker horizon close to 1600 ms through disorder volumes computed from the seismic data volume after preconditioning shown intersected by an arbitrary line from the seismic data volume. The high disorder lineaments seen on the display in Figure 10 are not seen as faults by the coherence. Data courtesy of Arcis Seismic Solutions, TGS, Calgary.

seismic volumes. Notice the low disorder values where the reflections are coherent and high values for not-so-coherent reflection zones. In Figures 8a and 8b, we show the corresponding images after structure-oriented filtering where the discontinuities are sharpened and cross-cutting noise is suppressed. Notice how the preconditioning alters the disorder-attribute display. Thus, we conclude that in the case of prominent faults, the disorder attribute is enhanced along the fault planes.

Having demonstrated this, we go back to our earlier example and exhibit similar results from that data set. In Figures 9a and

9b, we show strata slices through the disorder attribute before and after structure-oriented filtering. Again notice the enhanced signal-to-noise ratio as well as the sharpness of the faults after preconditioning. On the displays shown in Figures 10a and 10b, we now overlay the energy ratio coherence (seen in black) using transparency. We see the coherence lineaments exactly overlaying the fault indicated at A. However, the faults indicated at B and C have higher disorder values seen on both sides of the black coherence lineaments. We interpret such values as being indicative of fractures associated with the main faults with confidence. There are also some high disorder events seen on Figure 10b that are not seen as faults on the coherence overlay. To understand this, In Figure 11 we show the same strat slice exhibited in Figure 10b intersected by an arbitrary line from the seismic data. Notice there is no clear fault signature seen on the seismic corresponding to the high disorder event, but a disruption in the seismic reflection is definitely seen at the location of the yellow arrow.

Example 2

The next example is from a prestack depth-migrated data volume acquired in the Gulf of Mexico. Equivalent vertical slices are shown in Figures 12 and 13 through the seismic amplitude, disorder, and energy volumes. While a prominent salt dome is seen in the middle of the sections, notice that the outline of the salt body is not well-defined everywhere but can be interpreted easily using concepts of pattern recognition that differentiate the seismic response inside the salt dome from that outside the salt dome (Figure 12b).

Just outside the interpreted salt outline on the left and right of the dome, the seismic reflections are insufficiently imaged and appear as broken, somewhat chaotic, but relatively strong amplitude events highlighted by the light blue and light green polygons.
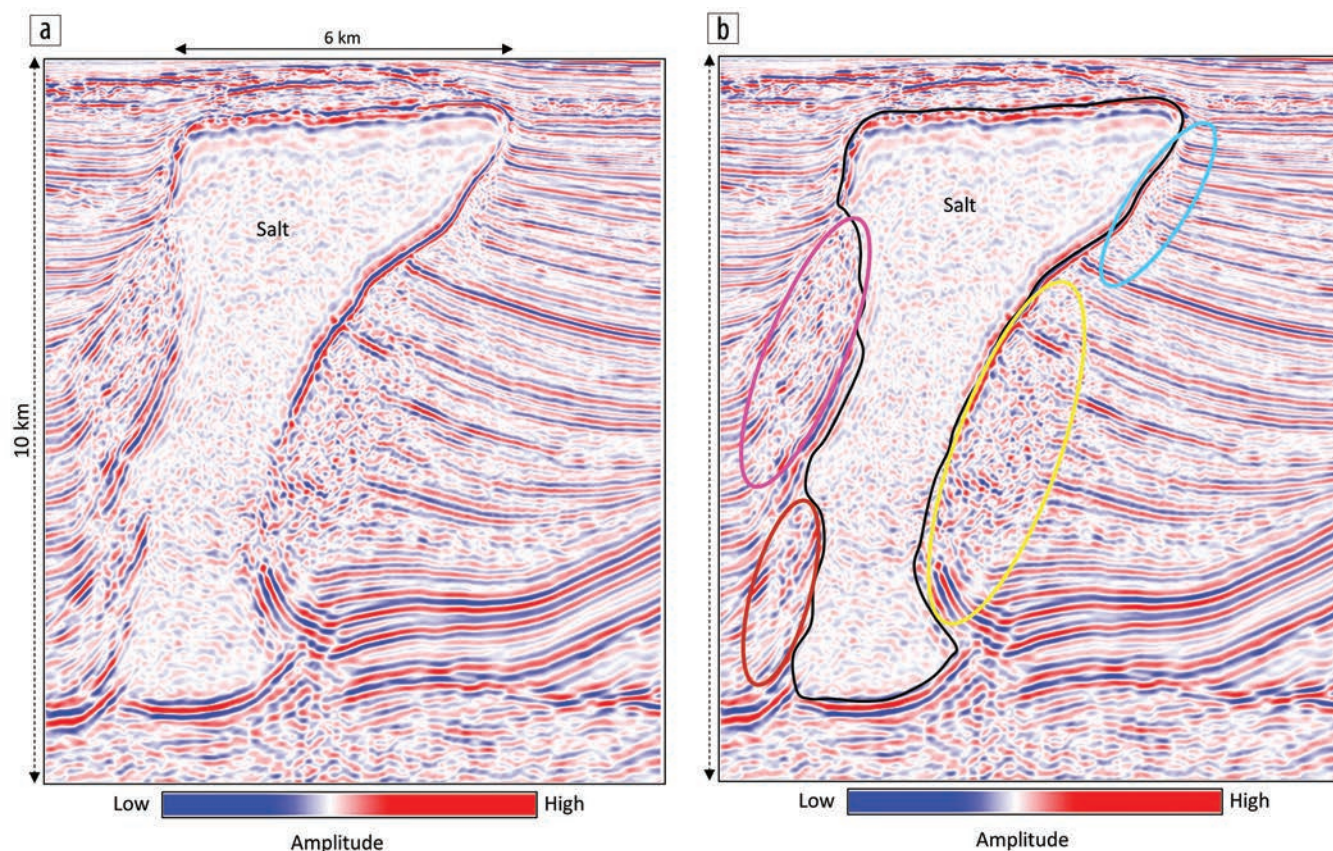
Figure 12. Segment of a seismic depth section (a) without and (b) with interpretation from the Thunderhorse area in the Gulf of Mexico showing a massive salt dome. The boundary of the dome is well-defined on the right, but on the left all we see are the abutting reflections. Low-amplitude chaotic reflections characterize the interior of the salt dome, while the poorly imaged chaotic reflectors outside the salt dome exhibit higher amplitude. Data courtesy of TGS, Houston.
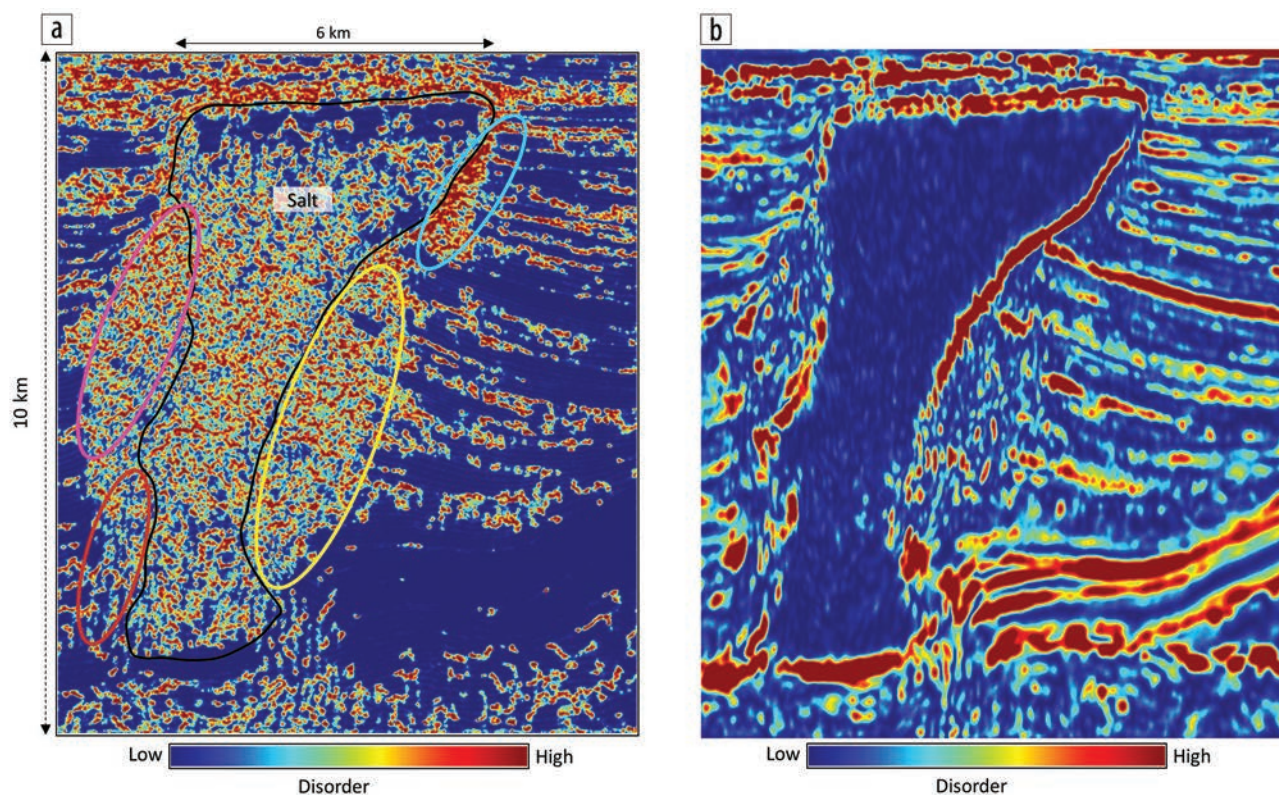

Figure 13. The same segment of the depth section shown in Figure 11 showing (a) disorder and (b) energy within a 50 m by 50 m by 50 m window. The body of the salt, as well as the areas in the highlighting ellipses exhibits low energy chaotic reflections which are can be distinguished from the high energy chaotic reflections outside the interpreted salt body. Data courtesy of TGS, Houston.

Accordingly, the disorder attribute points out higher values in these highlighted areas. In contrast, the chaotic (mostly noise) events inside the salt dome are lower in amplitude. To differentiate the two chaotic patterns, we need to add a second attribute, which is simply the total (unfiltered) energy of the input data within the analysis window (50 m by 50 m by 50 m), that is sensitive to the strength of these chaotic events (Figure 13b). A geobody can then be picked by corendering the two images.

In a similar way, the seismic disorder attribute can be used to map incoherent reflection packages such as mass-transport complexes and karst collapse features.

Conclusions

We have shown the application of seismic disorder attribute to two different data examples and have found that it is a useful attribute. By construction, the disorder attribute has a low response to sharp faults and coherent reflectors, but a higher response to more diffuse fault zones and incoherent reflectors. Structure-oriented filtering appears to enhance these damage zones. More quantitative assessment of such images will require horizontal image logs through diverse fault zones. **TLE**

Acknowledgments

References

Al-Dossary, S., Y. E. Wang, and M. McFarlane, 2014, Estimating randomness using seismic disorder: Interpretation, **2**, no. 1, SA93–SA97, http://dx.doi.org/10.1190/INT-2013-0088.1.

Bahorich, M., and S. Farmer, 1995, 3-D seismic discontinuity for faults and stratigraphic features: The coherence cube: The Leading Edge, **14**, no. 10, 1053–1058, http://dx.doi.org/10.1190/1.1437077.

Chopra, S., and V. Alexeev, 2005, Applications of texture attributes to 3D seismic data: CSEG Recorder, **30**, no. 7, 28–32.

Chopra, S., and K. J. Marfurt, 2008, Gleaning meaningful information from seismic attributes: First Break, **26**, no. 1292, 43–53, http://dx.doi.org/10.3997/1365-2397.2008012.

Chopra, S., S. Misra, and K. J. Marfurt, 2011, Coherence and curvature attributes on preconditioned seismic data: The Leading Edge, **30**, no. 4, 386–393, http://dx.doi.org/10.1190/1.3575281.

Chopra, S., and K. J. Marfurt, 2013, Preconditioning seismic data with 5D interpolation for computing geometric attributes: The Leading Edge, **32**, no. 12, 1456–1460, http://dx.doi.org/10.1190/tle32121456.1.

Dash, B. P., and K. A. Obaidullah, 1970, Determination of signal and noise statistics using correlation theory: Geophysics, **35**, no. 1, 24–32, http://dx.doi.org/10.1190/1.1440077.

Gao, D., 2003, Volume texture extraction for 3-D seismic visualization and interpretation: Geophysics, **68**, no. 4, 1294–1302, http://dx.doi.org/10.1190/1.1598122.

Ha, T., and K. J. Marfurt, 2014, Disorder attribute implementation on TX-LA dataset: Estimate horizon-picking confidence and map chaotic features, The University of Oklahoma, AASPI Annual Meeting.

Randen, T, S. I. Pedersen, and L. Sonneland, 2001, Automatic extraction of fault surfaces from three-dimensional seismic data: 71st Annual International Meeting, SEG, Expanded Abstracts, 551–554, http://dx.doi.org/10.1190/1.1816675.

West, B., S. May, J. E. Eastwood, and C. Rossen, 2002, Interactive seismic facies classification using textural attributes and neural networks: The Leading Edge, **21**, no. 10, 1042–1049, http://dx.doi.org/10.1190/1.1518444.